Available online at www.sciencedirect.com

SciVerse ScienceDirect

Procedia Engineering 58 (2013) 508 – 516

Procedia Engineering

www.elsevier.com/locate/procedia

The 12th Hypervelocity Impact Symposium

A New Online Resource for the Hypervelocity Impact Community and the Change of Debris Cloud Impact Patterns With Impact Velocity

K. Loft[a], M. C. Price[a,] *, M. J. Cole[a] and M. J. Burchell[a]

[a]*Centre for Astrophysics and Planetary Science, School of Physical Sciences, University of Kent, Canterbury,Kent, CT2 7NH, UK.*

Abstract

We announce the creation of a new online archive containing high resolution images, and measurements of over 200 metal plates impacted with a variety of projectiles at velocities between 1 and 8.5 km s^{-1}. This archive is being made freely accessible for use by the shock physics and hypervelocity impact research communities.
During the course of this archival work, it was discovered that debris cloud impact patterns from nylon projectiles form distinct geometric patterns, and that these patterns seem to fall into a distinct group depending on the projectile impact velocity. Complementary hydrocode modelling (using Ansys' AUTODYN) has been performed to try to recreate the patterns, but was not entirely successful, indicating that there is some physics that is not simulated within the hydrocode. Full details of the online archive and the hydrocode modelling are detailed in a much longer manuscript published by Loft K, Price M. C. *et al.* in the special HVIS 2012 edition of the *Int. J. of Impact Engineering* (DOI: 10.1016/j.ijimpeng.2012.07.007).

Keywords: aluminium; ballistic; hypervelocity; modelling; debris clouds.

1. Introduction

The Light Gas Gun (LGG) at the University of Kent [1] has been in operation for over 20 years and during that period thousands of different targets have been impacted with a variety of projectiles at a range of speeds between 1 – 8.5 km s^{-1}. During regular, routine maintenance shots to re-calibrate and re-configure the gun, a large number (in excess of 200) metal plates were impacted. Such shots were not part of an individual scientific project and the targets were archived and never analysed, thus providing a (currently) unexploited data resource.

After each shot, the plates were engraved with the shot ID, and (usually) with the witness plate configuration, projectile and impact velocity. The shot ID takes the form of a letter (normally 'G' or 'L') followed by the day, month, last two digits of the year and the shot number of the day. For example, 'G260411#2' would denote the second shot carried out on the 26th April 2011. If not part of a specific research programme, nothing further was done with the plates, and they were placed into storage.

Figure 1 is a photograph (top view) of a typical setup for a plate impact experiment. 'T' refers to the target plate, and W_1 and W_2 the witness plates (and W_3 if, rarely, a third witness plate is used). The relative distances behind the target plate of the witness plates are d_1 and d_2 respectively. The arrow on the left hand side of the image illustrates the impact direction. Target and witness plates were 100 mm × 100 mm square, and all aluminium plates were Al-6061.

* Corresponding author. Tel.: +44 1227 823594.
E-mail address: mcp2@star.kent.ac.uk

doi:10.1016/j.proeng.2013.05.058

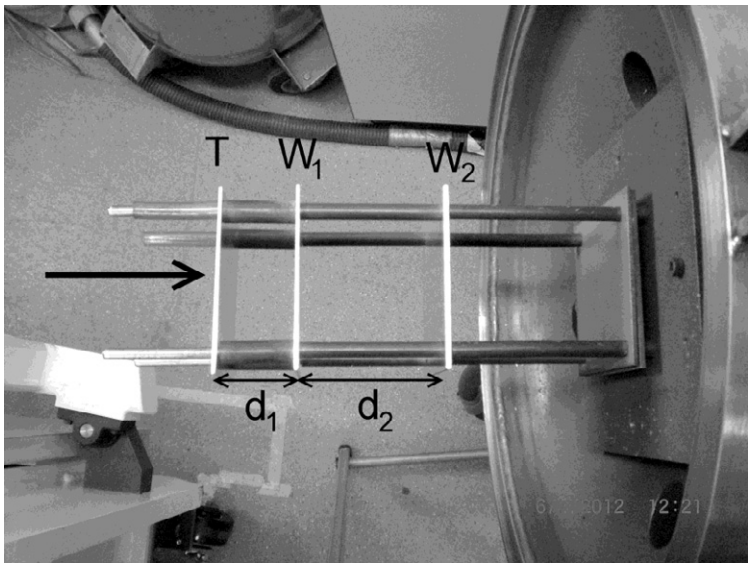

Fig. 1. Photograph showing a typical plate configuration before a shot. 'T' is the target plate, and W_1 and W_2 the witness plates. The relative distances between the plates are d_1 and d_2. In this example d_1 = 40 mm and d_2 = 80 mm. All plates are Al-6061 alloy; T and W_1 are 1.5 mm thick; W_2 is 3 mm thick. The arrow indicates the impact direction relative to the target plate.

1.1. Description of the archived data.

For each complete set of plates (target and associated witness plates) high resolution (9.1 megapixel – 3456 × 2592 pixels) images were taken of the front (impacted) surface, and the front surfaces of the witness plates. Additionally, low magnification (×7.1) microscope images were taken of the hole made by the projectile in the front of target plate. There are 400 images (to date) currently within the archive, with more to be added. Figure 2 is a montage of some example images, and in each case the projectile was a solid nylon cylinder with a diameter and length of 4.5 mm. Fig. 2A is an image of an entrance hole in a 1.5 mm thick aluminium plate impacted at a speed of 5.20 km s^{-1}. Fig. 2B is a photograph of a witness plate that was placed 100 mm behind a target plate. The projectile was travelling at 7.30 km s^{-1}. Note the spiral pattern formed by the impact of the debris cloud. Fig. 2C is a photograph of a witness plate that was placed 100 mm behind a target plate, with the projectile impacting at 6.32 km s^{-1}. This illustrates the discretisation of the ejecta pattern into radial lines. Fig. 2D is a photograph of a witness plate that was placed 100 mm behind a target plate and the projectile impacting at 5.05 km s^{-1} and illustrates the discretisation of the ejecta pattern into concentric rings.

Observations of similar patterns have been reported numerous times in the literature for glass and other impactors [2, 3 and 4]. For example, Hörz F. and co-workers describe such patterns in extensive detail in a series of papers [5, 6, 7, 8] as does Pietkutowski A. J. [9] in a comprehensive and in-depth description of the results from a programme of hypervelocity impact experiments. Theoretical and modelling work has also been done such as described in Zhang *et al.* [10] and Yattea *et al.* [11] and references therein. However, much of these data were obtained by varying the target plate thickness relative to the diameter of the (glass or aluminium) projectile. Within our dataset, we can see the change of the geometric patterns solely due to changing the impact velocity (and thus the maximum shock pressure).

In addition to the photographic record, for each set of plates the following data have been tabulated: entrance hole diameter, lip height above the front surface of target plate, projectile type, projectile speed, target plate thickness, witness plate distance(s) behind target plate, witness plate thickness(es). The complete dataset is tabulated in Appendix A for solid nylon cylindrical projectiles (Table A.1), stainless steel spherical projectiles (Table A.2) and other miscellaneous spherical projectiles (Table A.3)

2. Pattern descriptions

Here we confine our discussion to patterns associated with solid nylon projectiles impacting aluminium targets plates. Although similar patterns are seen with other projectile (and target plate) materials, there are (currently) insufficient data to infer if the observed patterns change as a function of impact velocity.

The patterns fall into four broad groupings: i) Random, ii) Concentric rings (referred to as 'hole-saw rings' by Hörz), iii) Spirals and iv) Radial lines, and are generally formed within a certain velocity regime, although overlaps do occur.

2.1.1 Random

These are observed at the lowest speeds (generally below 3 km s^{-1}) and consist of large, irregularly space 'pits' caused by ejecta impacting the witness plate. At the very lowest speeds, fragments of the nylon projectile survive intact and are seen as white fragments on the surface of the witness plate. Impact pressures at these speeds are relatively low (a few GPa), and are insufficient to cause impact melting of the target plate or projectile. An example is given in Figure 2A.

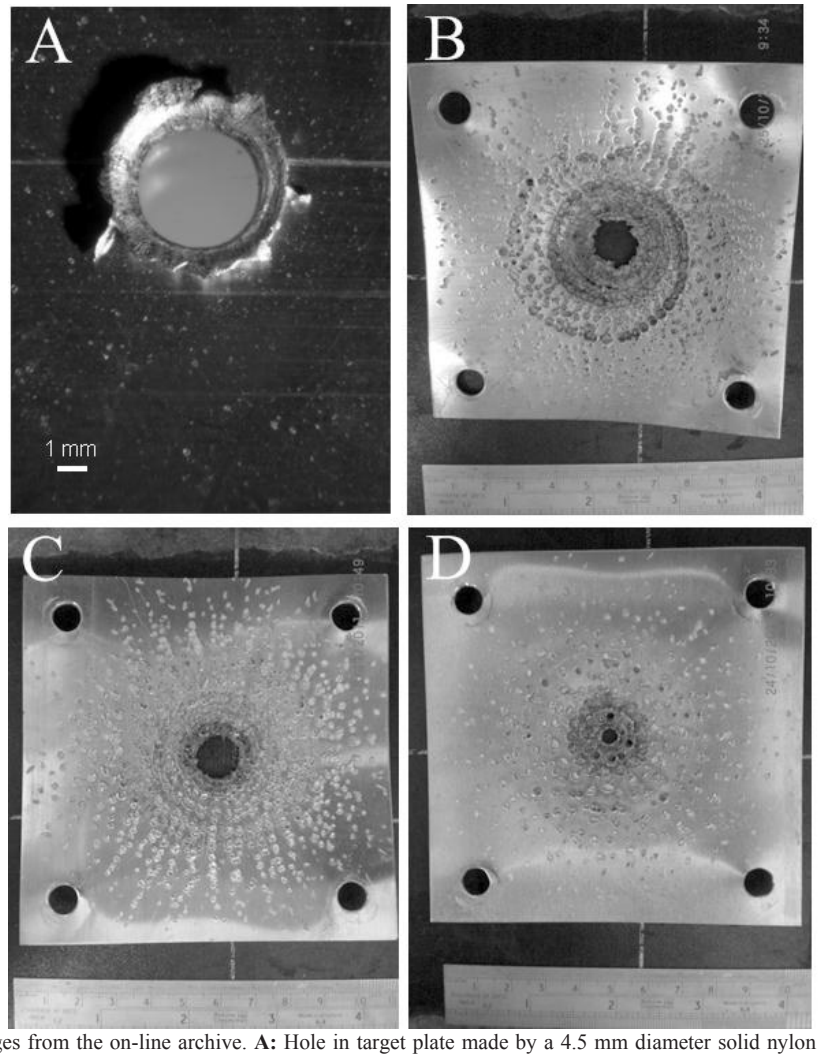

Fig. 2: Sample images from the on-line archive. **A:** Hole in target plate made by a 4.5 mm diameter solid nylon projectile travelling at 5.20 km s^{-1}. **B:** Spiral spall pattern on witness plate made by penetration of aluminium target plate by a 4.5 mm nylon projectile travelling at 7.30 km s^{-1}. **C:** Radial spall lines (and rings) made by penetration of aluminium target plate by a 4.5 mm nylon projectile travelling at 6.32 km s^{-1}. **D:** Concentric rings made by penetration of aluminium plate by a 4.5 mm nylon projectile at 5.05 km s^{-1}.

2.1.2 *Concentric rings*

Figure 2D gives an example of the concentric ring pattern from a high speed impact. The rings are generally centrally symmetric (although some deviations are observed) and start to occur at speeds above 2 km s^{-1}, starting to dominate over the 'Random' pattern with increasing velocity. At ~2 km s^{-1}, the number of rings is small (two or three) and consists of a coarse circular chain of relatively large craters. As the impact speed increases, the number of rings increases, with a subsequent

decrease in the size of the craters forming then. At speeds exceeding 5 km s^{-1}, hybrid patterns start to appear consisting of a mix of spiral, and concentric ring patterns.

2.1.3 *Spirals*

Spirals seem to occur in a limited velocity regime between 6 and 7.5 km s^{-1}. Above 7.5 km s^{-1}, 'Radial' (see below) patterns seem to dominate, but the statistics are poor, due to the small number of shots performed at the very highest speeds. Figure 2B is an example of a spiral pattern. It is theorised that the spiral pattern occurs due to the transfer of angular momentum from the molten nylon projectile (which is spinning due to the rifling of the gun barrel) to the molten target plate material. The number of twists in the spiral varies from three to five twists.

2.1.4 *Radial lines*

Radial lines patterns occur at all velocities above 2 km s^{-1}, but become more evident at higher velocities. They consist of an evenly spaced set of radial lines of craters emanating from the centre of the witness plate (Figure 2C). This is the dominant pattern observed at speeds above 7 km s^{-1}. Interestingly, the number of radial lines (referred to as 'spokes') seems to only vary between approximately 20 and 40.

2.2 Raman analyses of 'spider-web' filigree lines

As well as the geometric patterns observed, some witness plates had a fine filigree pattern, in addition to the more prominent ejecta patterns made by craters. An example of this is given in Figure 3, which shows the entire impacted witness plate (Fig. 3A), a zoomed (×10 magnification) section of part of the filigree ring pattern (Fig. 3B), and a Raman map (taken at a magnification of ×100). The white hatched area in Fig. 3C indicates the distribution of the Raman signature of nylon (see text and Fig. 4) demonstrating that the filigree pattern was made by (molten?) projectile material.

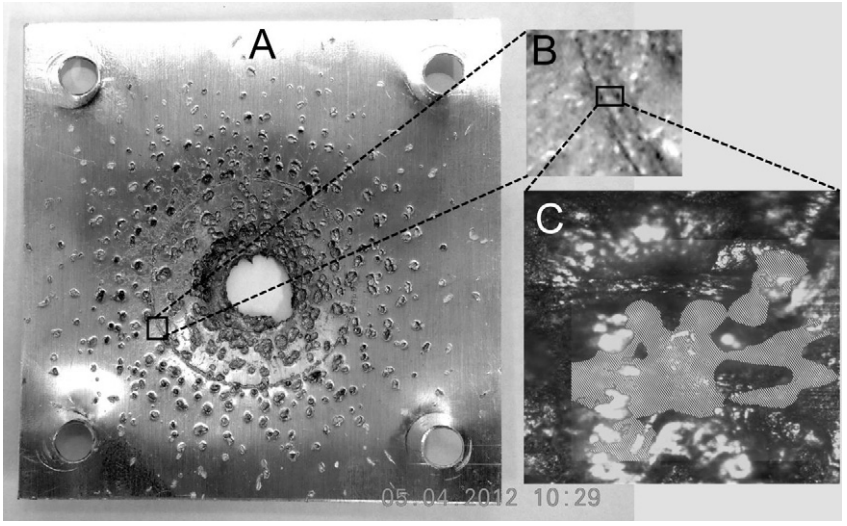

Fig. 3: Example of filigree pattern (thin ring in Fig. 3A); zoomed in (×10 magnification) section (Fig. 3B), and the distribution of nylon (white hatched areas in Fig. 3C, ×100 magnification) signifying that the filigree ring was made by molten nylon. The witness plate is 100 mm × 100 mm square and the impact speed was 5 km s^{-1}.

The difference in morphology between the fine filigree patterns and the surrounding cratering patterns, is very similar to that observed by Hörz *et al* (who refers to these features as 'projectile melt stringers'). Hörz demonstrated that the fine gouges observed in his witness plates were made by glass projectile melt via elemental mapping using energy dispersive X-ray spectroscopy (EDX). Here we also wished to verify that the filigree patterns we observe were also due to projectile melt, and not ejecta from the aluminium target plate. In order to achieve this, the plate shown in Fig. 3 was scanned with a mapping Raman spectrometer (Horiba *LabRam-HR* using a blue, 432 nm, excitation laser). Raman spectroscopy is very sensitive to the detection of organic species, and is ideal for tracing the distribution of organic impact residue [12]. Figure 4 (top trace) is an example Raman spectrum obtained from the area of filigree ring outlined in Fig. 3B. The two broad peaks

seen between 1200 and 1700 cm^{-1} are the distinctive 'D' and 'G' bands of elemental carbon, possibly due to contaminating soot from the gun and/or thermal decomposition of the nylon projectile. The broad line at 2900 cm^{-1} is due to C-H vibrational modes and indicates the presence of nylon, supported by the faint line at 1439 cm^{-1}. These match features seen in the Raman spectrum of a standard nylon projectile (bottom spectrum). The hatched region of Fig. 3C shows the distribution of the Raman signal strength of the hatched waveband (2800 – 2950 cm^{-1} – Fig. 4) and thus traces the presence of nylon within the filigree ring.

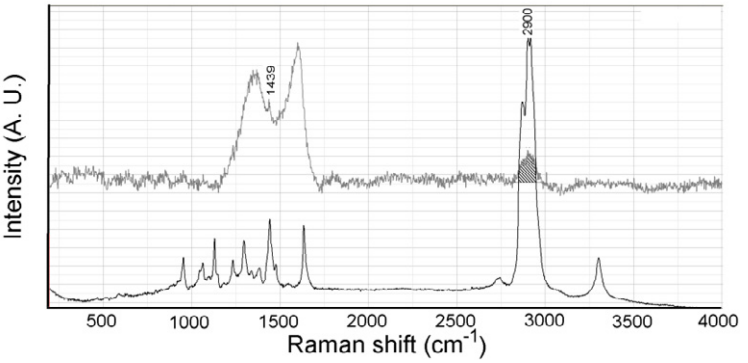

Fig. 4. Raman spectra of nylon. Top trace: Raman spectrum of impact residue in filigree ring show in Figure 3. Bottom trace: Raman spectrum of un-shot nylon sabot. The features at 2900 and 1439 cm^{-1} in the impact residue spectrum are 'fingerprint' indicators of nylon.

3. Ejecta pattern evolution as a function of impact speed.

3.1 Hydrocode modelling.

Hydrocode modelling using *Ansys'* AUTODYN (V12.1) was performed to try and replicate the range of patterns seen. Full details of this modelling, and comparison with the experimental data from the archive is presented in [16], Loft K., Price M. C. *et al* (IJIE special edition from HVIS 2012, DOI: 10.1016/j.ijimpeng.2012.07.007).

In summary, our modelling demonstrated:

1) AUTODYN reproduces the projectile hole diameter in an aluminium target plate to an accuracy of better than ±12%.

2) Cloud debris parameters such as velocity and lateral dimensions are modelled to within 10%.

3) The general trend of larger fragments at low velocities with smaller ejection angles is followed.

4) Even though projectile spin is modelled, no evidence is seen in the simulations of spiral debris patterns.

5) There is also no evidence of radial lines at any simulated velocity, although there is some evidence for the formation of concentric rings.

The last two points are of interest as the simulations do show melting of the target material as well as complete tensile failure of the projectile (resulting in fragmentation). If, as theorised, spiral patterns are formed from spinning molten droplets, then the hydrocode is failing to simulate this correctly. A standard SPH modelling approach does not allow merging of different materials into a single SPH particle, so mixing of melts cannot be easily simulated, possibly causing the failure to reproduce this pattern in the simulations. Additionally, the calculation above may indicate that the formation of the spirals is more complicated than simple momentum transfer from the projectile to the target.

As far as the authors are aware, it is unknown what mechanism causes the radial patterns observed. During a high velocity impact (>6 km s^{-1}) a plasma cloud is formed in front and behind the target plate. It is possible that as pressure waves travel through this cloud then pressure nodes and anti-nodes are produced which may 'shepherd' the ejecta material into regularly spaced regions resulting in the regular geometric patterns observed. As the hydrocode does not simulate the production of the impact plasma, then it could not reproduce the radial patterns.

4. Conclusions

With the increasing need to investigate the best shielding configuration to guard spacecraft against probable catastrophic impacts, from man-made and (natural) impactors, due to the rise of space debris in near-earth orbit, [13] it is hoped that this resource will complement ongoing impact experiments by other researchers. Additionally it provides a large dataset to help in the validation of hydrocodes, such as that described here and instigated by Pierazzo *et al*. [14] as well as data for the refinement of ballistic limit equations [15].

Additionally, the intriguing changes observed in the debris cloud patterns described herein, and which are not reproduced with within AUTODYN, give insight into shock wave propagation, melting, and the interaction of that melt within targets and projectiles. Further work is ongoing into quantifying the debris cloud patterns observed, specifically including a more exact quantification of the number of spokes observed in radial patterns and number of twists in a spiral pattern.

The archive

The URL for the archive is http://astro.kent.ac.uk/target_archive and is password protected. Potential users of the archive should e-mail mcp2@star.kent.ac.uk to request a login.

Acknowledgements

The authors thank SERC, PPARC and now the STFC, UK for funding impact experiments at the University of Kent for the past 20 years.

References

[1] Burchell M. J. et al. (1999). "Hypervelocity impact studies using the 2 MV Van de Graaff accelerator and two-stage light gas gun of the University of Kent at Canterbury".*Measurement Science & Technology* **10**, 41 - 50.
[2] Schonberg W. P. & Taylor R. A. (1989). "Penetration and ricochet phenomena in oblique hypervelocity impact". *AIAA Journal,* **27**, 639 - 646
[3] Stilp A. J. et al. (1990). "Debris cloud expansion studies". *International Journal of Impact Engineering,* **10**, 543 – 554.
[4] Pietkutowski A. J. (1990). "A simple dynamic model for the formation of debris clouds". *International Journal of Impact Engineering,* **10**, 453 – 472.
[5] Hörz F. et al. (1995). "Penetration Experiments in Aluminum 1100 targets using soda-lime glass projectiles". *NASA Technical Memorandum* No. 104813.
[6] Hörz F. et al. (1994). "Dimensionally scaled penetration experiments: aluminum targets and glass projectiles 50 μm to 3.2 mm in diameter". *International Journal of Impact Engineering,* **15**, 257 – 279.
[7] Hörz F. et al. (1997). "Evolution of debris plumes as inferred from witness plates". *International Journal of Impact Engineering,* **20**, 387 – 398.
[8] Gwynn D. W et al. (1997). "The dispersion of molten soda-lime glass projectiles following penetration of thin aluminium membranes". *International Journal of Impact Engineering* **20**, 325 – 336.
[9] Pietkutowski A. J. (1996). "Formation and description of debris clouds produced by hypervelocity impact". *NASA technical report (UDR-TR-95-46),* University of Dayton Research Institute, for NASA Marshall Space Flight Center, MSFC, Alabama, NASA CR 4707.
[10] Yatteau J. D., Wilson L. T. and Dickinson D. L. (2010). "Assessment of FATEPEN for application to spacecraft micrometeoroid and orbital debris penetration analyses". *Proceedings of the 11th Hypervelocity Impact Symposium,* 260 - 274.
[11] Zhang Q. M., Chen Y.H. and Huang F.L. (2010). "The expansion model of debris cloud induced by oblique hypervelocity impact". *Proceedings of the 11th Hypervelocity Impact Symposium,* 352 - 365.
[12] Price M. C. et al. (2012)**.** "Alteration and formation of organic molecules via hypervelocity impacts". *43rd Lunar and Planetary Science Conference,* Abstract #1755.
[13] Liou J. C. & Johnson N. L. (2006). "Risks in Space from Orbiting Debris", *Science*, **311**, 5759, 340.
[14] Pierazzo et al. (2008). "Validation of numerical codes for impact and explosion cratering: Impacts on strengthless and metal targets". *Meteoritics and Planetary Science,* **43,** 1917 – 1938.
[15] Ryan S. et al. (2008). "A ballistic limit equation for hypervelocity impacts on composite honeycomb sandwich panel satellite structures", *Advances in Space Research*, **7**, 115.
[16] Price M. C. et al. (2012). "Impacts into metals targets at velocities greater than 1 km/sec: a new online resource for the hypervelocity impact community and an illustration of the geometric change of debris cloud impact patterns with impact velocity". *International Journal of Impact Engineering (HVIS 2012 special edition, in press),* DOI: 10.1016/j.ijimpeng.2012.07.007.

Appendix A: Tables of results from all plates currently in the online archive. Note, a empty cell, or '-', indicates unknown, or missing data.

Table A1: Details of analysed results from measurements of plates impacted by solid nylon, cylindrical, sabots. Notes: **a)** Shot ID as found engraved on plates**.**
b) Two standard calibres of barrel are used for shots: 0.177" and 0.22".**c)**As measured with a low power microscope. Two measurements in a cell indicate that there were two holes in the target plate (a second hole is occasionally made by the punched out centre of the bursting disk travelling down the range). **d)** As measured with digital callipers. **e)** Witness plate configuration refers to the respective distance behind the target plate. Multiple witness plate distances are denoted as '40 + 80' meaning W_1 was 40 mm behind target plate and W_2 was 80 mm behind W_1.

Shot ID[a]	Projectile diameter (inches)[b]	Velocity (km s^{-1})	Target plate thickness (mm)	Hole inner diameter[c] (mm)	Hole inner diameter[d] (mm)	Lip-to-lip diameter (mm)	Lip height (mm)	Witness plate(s) thickness (mm)	Witness plate configuration[e] (mm)	Notes
G020409#1	0.22	1.32	1.5	8.64	8.40	10.45	0.23	3.0	78	
G251010#1	0.22	1.48	1.5	8.84	8.88	10.40	0.28	1.5	79	
G011110#1	0.22	1.55	1.5	9.78	9.56	10.93	0.45	1.5	79	
G240609#1	0.22	1.89	1.5	9.82	9.47	11.77	0.11	3.0	50	
G051108#1	0.22	1.93	1.5	9.65	9.59	11.56	0.21	1.5, 3.0	40 + 50	
G180609#3	0.22	1.98	1.5	9.88	9.80	11.80	0.81	3.1	50	
G020409#3	0.22	2.75	1.5	11.12	11.04	19.35	0.36	3.0	78	
G180609#2	0.22	2.79	1.5	11.04	10.81	13.34	0.84	1.5, 3.0	50 + 79	
G190509#1	0.22	2.90	1.5	11.28	11.15	13.78	0.67	1.5, 3.0	50 + 100	
G070409#1	0.22	2.99	1.5	11.25	10.92	13.22	0.63	3.0	78	
G190509#2	0.22	3.06	1.5	11.58	11.25	13.49	0.82	3.0	50	
G030609#1	0.22	3.09	1.5	11.45	11.26	13.19	0.84	3.0	78	
G150708#1	0.22	3.16	1.5	10.76	11.14	12.58	0.72	1.5, 1.5	40 + 50	
G070409#2	0.22	3.17	1.5	11.47	11.10	13.36	0.43	3.0	78	
G300409#1	0.22	3.31	1.5	11.64	11.53	14.23	0.86	3.1	78	
G200111#1	0.22	1.85	3.0	9.64 1)12.26	9.61 1) 12.31	11.56	0.74	1.5	80	
G110609#1	0.22	3.11	3.0	2) 9.80	2) 10.22	14.65	1.77	3.0		
G110609 #3	0.22	3.12	3.0	12.23	12.22	14.23	1.99	3.0	79	
L240299#1	0.177	1.81	1.5	9.82	9.69	12.86	1.84	1.5, 1.5, 1.5		
G061108#1	0.177	2.14	1.5	8.85	8.67	11.37	0.46	1.5, 1.5	40 + 80	
L261198#1	0.177	3.49	1.5	9.87	9.59	11.72	0.65	1.5	60	
L261198#2	0.177	4.51	1.5	10.46	10.13	12.40	0.75	1.5	60	
L261198#3	0.177	4.66	1.5	10.39	10.33	12.34	0.85	1.5		3rd plate missing
G041002#1	0.177	5.00	1.5	11.44	11.25	13.20	1.08	1.5, 3.0	40 + 80	Concentric
G110105#1	0.177	5.05	1.5	10.77	10.50	12.78	0.65	1.5	80	
L261198#4	0.177	5.32	1.5	10.85	10.55	12.57	0.76	1.5		Possible 3rd Plate
L070999#1	0.177	5.58	1.5	11.74	11.48	13.92	0.89	1.5	122	
L140999 #3	0.177	5.62	1.5	11.58	11.43	13.47	0.92	1.5	120	
020506#3	0.177	5.67	1.5	11.89	11.89	13.84	1.03	3.0		
L270498#3	0.177	5.68	1.5	11.62	11.60	13.94	1.21	1.5	100	Burst disk impact
270498#4	0.177	5.70	1.5	12.02	11.61	14.22	0.81	3.0	100	
G041002#2	0.177	5.73	1.5	11.81	11.63	13.45	1.13	1.5	40	3rd Plate missing, Burst disk impact
131099#1	0.177	5.82	1.5	11.85	11.48	13.86	0.93	3.0	60	
G200303#1	0.177	5.88	1.5	11.63	11.60	13.57	0.97	1.5, 3.0	40 + 80	Radial
L140999#4	0.177	5.92	1.5	11.94	11.60	13.84	1.05	1.5	120	Concentric
L070999#2	0.177	6.01	1.5	12.02	11.79	14.34	0.95	1.5	122	
G210303#1	0.177	6.11	1.5	11.53 1) 11.76	11.74 1) 11.73	13.14	1.01	1.5, 3.0	40 + 80	Spiral Burst disc impact.
G170403#1	0.177	6.14	1.5	2) 13.18	2) 13.59	13.59	1.06	1.5, 3.0	40 + 80	Spiral/radial (?)
L171198#3	0.177	6.24	1.5	12.17	11.87	14.14	0.82	2.0		
G280303#1	0.177	6.32	1.5	11.57	11.71	13.35	1.23	1.5, 1.5	40 + 80	Radial
L140999#1	0.177	6.37	1.5	12.12	11.85	14.51	0.96	1.5	120	
G080301#3	0.177	6.48	1.5	11.95	11.98	13.71	0.88	3.0	150	Concentric
051099#1	0.177	6.53	1.5	11.74	11.80	13.60	0.95	3.0	60	
G280303#2	0.177	6.56	1.5	11.66	11.67	13.70	0.97	1.5, 3.0	40 + 80	Radial
L140999 #2	0.177	6.59	1.5	12.00	11.92	14.14	1.14	1.5	120	
L240999 #1	0.177	6.60	1.5	12.00	11.92	14.41	1.01	2.9	60	
G041002#3	0.177	6.61	1.5	12.12	11.95	14.22	1.20	3.0	40 + 80	Odd pattern. Hybrid (?)
L011099#1	0.177	6.63	1.5	12.17	12.00	14.47	1.13	3.0	60	
051099#2	0.177	6.70	1.5	11.95	12.00	14.17	0.99	3.0	60	
G060605#2	0.177	6.70	1.5	11.28	11.25	13.16	0.82	1.5, 3.0	40 + 80	Radial
G280303#4	0.177	6.72	1.5	12.07	11.99	14.24	1.19	1.5, 3.0	40 + 80	
G280303#3	0.177	6.76	1.5	11.99	12.08	14.24	1.00	1.5, 3.0	40 + 80	
G071002#1	0.177	6.78	1.5	12.18	11.94	14.18	0.97	1.5, 3.0	40 + 80	
L240999#2	0.177	6.79	1.5	12.28	12.05	14.40	1.18	3.0		
L051099#3	0.177	6.86	1.5	11.85	11.83	13.44	1.00	3.0	60	

G181002#1	0.177	6.99	1.5	12.37	12.17	14.64	1.21	1.5, 3.0	40 + 80	Weak spiral
G160802#1	0.177	7.03	1.5	12.28	12.10	14.53	0.92	1.5, 3.0	120	Burst disk impact
G071002#2	0.177	7.04	1.5	12.10	12.06	14.19	1.03	1.5, 3.0	40 + 80	
G160902#1	0.177	7.05	1.5	12.45	12.14	14.90	0.99	3.0	120	
G070605#1	0.177	7.06	1.5	11.50	11.47	13.86	0.78	1.5, 3.0	40 + 80	
G280403#1	0.177	7.10	1.5	12.06	12.06	14.11	1.06	1.5, 3.0	40 + 80	Spiral
G071002#3	0.177	7.19	1.5	11.69	12.22	13.43	1.06	1.5,3.0	40 + 80	Bent radial. Hybrid (?)
L011099#2	0.177	7.19	1.5	12.40	12.16	14.91	1.09	3.0	60	
G070605#3	0.177	7.20	1.5	1) 10.05 2) 5.27	1) 9.95 2) 5.35	10.75	0.39	1.5, 3.0	40 + 80	Burst disc impact
G171002#2	0.177	7.22	1.5	12.49	12.16	14.80	1.36	1.5, 3.0	40 + 80	Spiral
L011099#3	0.177	7.27	1.5	12.41	12.16	14.83	1.11	3.0	60	
G171002#1	0.177	7.28	1.5	12.49	12.24	14.84	1.14	1.5, 3.0	40 + 80	Weak radial
G070605#2	0.177	7.30	1.5	11.61	11.58	13.68	0.69	1.5, 3.0	40 + 80	Odd pattern. Hybrid (?)
G241002#2	0.177	7.30	1.5	12.35	12.1	14.24	1.03	1.5, 3.0	40 + 80	Spiral
G251002#2	0.177	7.43	1.5	12.55	12.2	14.42	1.06	1.5, 3.0	40 + 80	Odd pattern. Hybrid (?)
G080103#4	0.177	7.48	1.5	1) 12.29 2) 12.80	1) 12.24 2) 12.17	14.28	0.68	1.5, 1.5	50 + 100	Burst disc impact
G280403#2	0.177	7.56	1.5	12.01	12.15	14.46	1.05	1.5, 3.0	40 + 80	Radial
G170103#3	0.177	7.70	1.5	12.15	12	14.22	1.19	1.5, 1.5	50 + 100	Odd pattern
G290403#1	0.177	7.73	1.5	12.12	11.98	14.38	1.12	1.5, 3.0	40 + 80	Radial
G090503#4	0.177	7.82	1.5	10.13	10.28	10.97	0.47	1.5, 3.0	40 + 80	Radial
G270203#2	0.177	7.94	1.5	12.00	11.91	14.32	0.92	1.5, 3.0	40 + 80	Radial/concentric
G270203#3	0.177	8.38	1.5	11.48	11.51	13.72	0.47	1.5, 3.0	40 + 80	Radial
L080699 #1	0.177	4.76	1.6	11.48	11.37	14.20	0.88	2.0	130	
L080699 #3	0.177	5.71	1.7	12.27	12.22	13.40	1.08	1.7	130	
L171198#4	0.177	5.42	2.0	13.16	12.76	15.36	1.22	1.5		
L040495#1	0.177	3.80	3.0	13.53	13.21	15.83	1.83	1.5		
G281005#2	0.177	~5.0	3.0	14.59	14.42	16.68	1.93	3.0	50	
G111105#1	0.177	~5.0	3.0	14.24	14.06	16.05	1.96	3.0	40	
G260107#3	0.177	5.04	3.0	11.15	11.57	12.89	0.63	3.0	40 + 50	
200198#3	0.177	5.19	3.0	13.98	13.65	16.08	2.15	3.0	?	
L171198#2	0.177	6.42	3.0	-	-	-	-	3.0	-	
G190503#2	0.177	6.79	3.0	15.30	15.40	-	2.17	3.0	40	
G190503#3	0.177	7.06	3.0	15.47	15.82	-	2.13	3.0	40	
G190902#1	0.177	7.09	3.0	-	-	-	1.82	3.0	120	
300693 (L020793?)	0.177	~5.0	3.4	12.91	12.81	1.57	1.62	3.3	120	

Table A2: Details of analysed results from measurements of plates impacted by stainless steel spheres. Notes: [a] Shot ID as found engraved on plates. [b] As measured with a low power microscope. Two measurements in a cell indicate that there were two holes in the target plate. [c] As measured with digital callipers. [d] Witness plate configuration refers to the respective distance behind the target plate. Multiple witness plate distances are denoted as '40 + 80' meaning W_1 was 40 mm behind target plate and W_2 was 80 mm behind W_1.

Shot ID[a]	Projectile diameter (mm)	Velocity (km s^{-1})	Target plate thickness (mm)	Inner hole diameter[b] (mm)	Inner hole diameter[c] (mm)	Lip-to-lip diameter (mm)	Lip height (mm)	Witness plate(s) thickness (mm)	Plate configuration (mm)[d]	Notes
G131210#1	1.0	1.16	1.5	1.23	1.15	1.60	0.17	3.0	50	
G061011#4	1.0	1.19	1.5	1.20	1.11	3.06	0.21	3.0	50	
G061011#2	1.0	1.19	1.5	1.36	1.1	1.66	0.21	3.0	50	
G061011#1	1.0	1.21	1.5	1.20	1.14	1.62	0.22	3.0	50	
G080212#2	1.0	3.95	1.5	3.15	3.39	3.95	0.98	3.0	40	
G030203#2	1.0	4.75	1.5	4.00	4.82	6.80	1.09	3.0	150 + 150	W_1 missing?
G081104#3	1.0	4.76	1.5	3.68	3.61	4.87	0.72	3.0	80	
G030203#1	1.0	4.80	1.5	3.90	3.98	5.06	0.93	3.0	150 + 150	W_1 missing?
L020398 #2	1.0	4.93	1.5	1) 8.42 2) 4.15	1) 8.33 2) 4.04	1) 10.01 2) 5.05	1) 1.24 2) 1.04	3.0	50	Burst disc impact
G170604#1	1.0	4.99	1.5	3.92	3.76	4.98	0.93	1.5	78	
G180105#4	1.0	5.02	1.5	1) 3.66 2) 1.06	1) 3.71 2) 1.50	4.86	0.855	1.5, 3.0	40 + 80	Burst disc impact?
L020398 #3	1.0	5.12	1.5	4.22	4.09	5.41	1.065	3.0	50?	
G060306#1	1.0	5.17	1.5	4.28	4.24	5.20	1.06	3.0	80	
G110105#2	1.0	5.21	1.5	3.85	3.78	5.05	1.035	3.0	80	
G141206#1	1.0	5.71	1.5	4.77	4.75	5.88	1.75	1.5, 3.0	Contact + 50	
G020407#2	1.0	5.95	1.5	4.12	4.51	4.91	1.27	3.0	100	

G080103#2	1.0	2.46	3.0	2.64	2.6	3.46	0.68	3.0	80	
G080103#1	1.0	2.78	3.0	3.08	2.97	3.85	0.83	3.0	80	
L020398 #1	1.0	4.65	3.0	4.07	4	5.21	0.96	1.5	50	
G020212#2	1.0	6.05	3.0	4.63	4.76	6.12	1.02	3.0	80	
G080212#1	1.0	7.36	3.0	4.70	5.16	5.94	1.63	3.0	40	
G090603#1	0.8	7.01	1.5	4.52	4.31	5.71	1.31	3.0	41	
G240209#1	1.5	6.03	1.5	5.89	5.94	7.36	0.98	3.0	100	
L090497#2	2.0	4.33	1.5	1) 6.23 2) 5.08	1) 6.31 2) 5.10	1) 7.52 2) 6.36	1) 1.32 2) 0.73	1.5	50	Burst disc impact
L110497#1	2.0	4.52	1.5	5.38	5.39	6.80	-	1.5	50	
G120106#1	2.5	4.59	3.0	8.88	9.17	11.43	2.48	3.0, 3.0	40 + 80	
G270203#1	3.0	7.67	1.5	11.62	11.75	13.56	0.75	1.5, 3.0	40 + 80	
G150808#1	1.0	6.23	1.0	4.16	4.16	5.12	1.02	1.5	100	Copper target plate

Table A3: Results from measurements of plates impacted by miscellaneous projectiles. Notes: [a] Shot ID as found engraved on plates**.** [b] Projectiles were spherical unless stated otherwise. [c]As measured with a low power microscope. Two measurements in a cell indicate that there were two holes in the target plate. [d] As measured with digital callipers. [e] Witness plate configuration refers to the respective distance behind the target plate. Multiple witness plate distances are denoted as '40 + 80' meaning W_1 was 40 mm behind target plate and W_2 was 80 mm behind W_1.

Shot ID[a]	Projectile type[b]	Projectile diameter (mm)	Target plate thickness (mm)	Velocity ($km s^{-1}$)	Inner hole diameter (mm)[c]	Inner hole diameter (mm)[d]	Distance Behind (mm)[e]
G180105#5	Copper	1.0	1.5	5.07	3.80	3.79	40 + 80
260603#3	Halite buckshot + copper	1.0	1.5	4.86	3.09	2.98	40
G240810#3	Copper	2.0	3.0	5.36	8.09	8.04	30
G240510#4	Copper	2.0	3.0	5.48	8.01	8.12	30
G031202#2	Ceramic	1.5	1.5	4.80	3.28	3.30	100
G221102#2	Ceramic	1.5	1.5	4.76	4.80	4.68	100
260603#2	Ceramic	1.5	1.5	4.60	1.61	1.64	40
260603#2	Ceramic	1.5	1.5	4.85	2.56	2.46	40
G101202#2	Ceramic	1.0	1.5	7.20	3.62	3.60	196
G271102#2	Ceramic	2.0	1.5	4.82	4.96	4.78	100
G161202#4	Ceramic	1.0	1.5	7.31	4.86	4.60	50
201099#2	Aluminium	1.0	3.0	5.45	5.70	5.63	-
G220311#3	Aluminium	3.0	3.0	5.81	10.33	10.31	In contact